Numerical estimation of the mode I strain energy release rate in woven-ply thermoplastic-based composites at high temperature based on Gθ method

M. Chabchoub, Benoît Vieille, Rostand Moutou Pitti

HAL Id: hal-02116817
https://hal.science/hal-02116817

Submitted on 22 Oct 2021

Numerical estimation of the mode I strain energy release rate in woven-ply thermoplastic-based composites at high temperature based on G_θ method

M. Chabchoub[a], B. Vieille[a], R. Moutou Pitti[b]

[a] Normandie Univ, UNIROUEN, INSA Rouen, CNRS, Groupe de Physique des Matériaux, 76801 St Etienne du Rouvray, France

[b] Université Clermont Auvergne, CNRS, Institut Pascal, 63000 Clermont-Ferrand, France

* Address correspondence to: Benoit.Vieille@insa-rouen.fr

Abstract

The present work was aimed at estimating the mode I strain energy release rate at crack initiation in woven-ply thermoplastic (TP) based laminates at high temperature $T > T_g$. A linear spectral viscoelastic model and a generalized Norton viscoplastic model were used to account for the time-dependent behavior of TP-based composite laminates, which are exacerbated at high temperature. To precisely evaluate the fracture parameters (e.g. R-curves) in TP composites, a study on the mesh type and its refinement was carried out. Using the finite element code Cast3m, the G_θ method was applied in order to test its capability to determine the mode I strain energy release rate for different testing conditions. 5-Harness satin weave carbon fabric reinforced PolyPhenylene Sulfide (5HS C/PPS) laminates have been studied with two different stacking sequences: a Quasi-Isotropic (QI) sequence characterized by a fibre-dominated behaviour and an Angle-Ply (AP) sequence whose behaviour is matrix-dominated. Tensile tests have been simulated on Single-Edge-Notch (SEN) specimens (with different notch lengths) subjected to quasi-static loadings in order to investigate the effect of time-dependent behaviors on translaminar failure and strain energy release rate. The R-curves have been derived from the computation of the strain energy release rate and the corresponding crack length. Ultimately, it is possible to build R-curves

based on the evaluation of fracture toughness for different ratios a/w and to compare these curves to the ones obtained from experiments.

Keywords: Thermoplastic-based composites; high temperature; translaminar fracture; strain energy release; G_θ method; numerical modelling.

I.   Introduction

The generalization of composite materials (50% mass ratio in recent aircrafts) in aeronautical structures raises issues at various levels: design, manufacture, assembly and control in service. Thus, the increasing use of composites has highlighted the limits of TS resins predominantly used in aeronautics. In addition, manual draping of TS prepregs is a well-controlled, but long and expensive process. Several manufacturing processes offer an alternative to manual draping of TS prepregs: Resin Transfer Molding, infusion, compression molding of thermoplastics. The constraints associated with TS have thus promoted the emergence of new materials Carbon fiber composites and high performance thermoplastic resin (TP) with a better compromise. If this type of polymer has been put aside for a long time due to poor mechanical properties at high temperature (i.e. about 120°-200°C for polymer matrix composites), the development of high performance resins (PEEK, PES, PI, PPS) in the 1990s, opened the door to structural composites combining carbon fibers and high-performance TP matrices. However, the use of polymer matrix composites (PMC) raises several problems concerning their large-scale exploitation in the aeronautics sector in terms of manufacturing (Stamping, RTM, Sheet Molding Compound, interpenetration welding of surface layers, etc.), behavior (under monotonic or cyclic loading), properties under critical conditions and more particularly their fracture behavior at high temperature.

I.1 Fracture mechanics in composite materials

There are different ways to approach fracture mechanics: locally through stress and strain fields around the crack tip, and more globally with the energy release rate (associated with material toughness). Depending on the material behaviour (e.g. linear elastic or elastic-plastic), different fracture mechanics frameworks can be considered. Thus, the determination of G-R (brittle fracture) and J-R curves (ductile fracture) is the key point to quantify fracture in terms of energy required to grow a crack in laminates with different lay-ups. In elastic brittle composite materials, fracture is usually analyzed by using the Linear Elastic Fracture Mechanics (LEFM) parameters: R-curve analysis, critical strain energy release rate G_{Ic}, stress intensity factor K_{Ic}. In elastic-ductile composite materials, fracture analysis is conducted by means of Elastic Plastic Fracture Mechanics (EPFM): J-integral, crack opening displacement or J-R curves. The knowledge of the R-curves is therefore of the utmost importance in composite materials design as it represents the energy brought to the material to extend a crack in heterogeneous and anisotropic media. This energy is directly associated with damage mechanisms resulting from composite materials' fracture toughness. In fibers reinforced polymer composites, the energy dissipated during controlled crack propagation is usually evaluated in terms of different energy-absorbing mechanisms: fiber breakage, local plastic deformation, matrix-cracking, fiber/matrix debonding and fiber pull-out [1-2]. In composite laminates, failure is determined by the combination of loading, location of defect and material heterogeneity (presence of matrix-rich regions at the crimp area in woven-ply laminates). When failure is initiated from an existing notch, a sequence of energy absorbing events occurs in a region surrounding the notch tip. The knowledge of energy-absorbing processes is therefore important since they are responsible for the toughness of the composite. Depending on laminates' stacking sequence, the contribution of matrix behavior to strain energy release rate can be evaluated during damage in both brittle and ductile composite laminates subjected

to high temperature conditions (T > Tg) when matrix ductility and toughness are enhanced [3-4]. In composite materials with a brittle matrix, the energies dissipated during crack initiation and propagation in the composite with a weak fiber/matrix interface are derived principally from the work of fiber pull-out (which is due to the frictional forces that hold a broken fiber in its matrix socket). In ductile matrix composite systems, the local plastic deformation of the matrix also must be taken into account to determine the total fracture toughness [5-6]. The fracture behavior (and therefore the fracture toughness) of TP polymers exhibits temperature dependence (viscoelastic and viscoplastic behaviors) not only above T_g but also below T_g. Kim et al. have studied the influence of temperature on the interlaminar failure of composites with TP coated carbon fibers [4]. Vieille et al. have studied the evolution of mode I translaminar failure along with the strain energy release rate at high temperature in carbon fibers reinforced PolyPhenylene Sulfide (PPS) composites [3-4].

I. 2 Fracture toughness of TP-based composites

When it comes to damage tolerance, high-performance TP matrix laminates are characterized by high values of fracture toughness compared to thermosetting-based composites. In addition, potential advantages of using woven-ply laminates as opposed to UD-ply laminates are discussed in the literature as woven-ply composites have higher values of interlaminar critical strain energy release rates G_{IC}. Most of the studies available in the literature deal with the mode I interlaminar failure of TP based composites by means of double cantilever beam tests. In orthotropic or quasi-isotropic composite laminates, transverse matrix cracking and fibers breakage (also known as translaminar failure modes) are usually the primary damage mechanisms occurring in the early phase of mechanical loading [3]. To the author's best knowledge, there is no study in the literature quantifying the influence of time-dependent behaviours on translaminar fracture of woven-ply composites. In the present study, 5-Harness

Satin weave carbon fabrics reinforced PolyPhenylene Sulfide (5HS C/PPS) laminates have been studied with two different stacking sequences: a Quasi-Isotropic (QI) sequence displaying a fibre-dominated behaviour and an Angle-Ply (AP) sequence with a matrix-dominated behavior [7]. It is expected that QI specimens show weak time-dependency in contrast to AP specimens. Tensile tests have been carried out on Single-Edge-Notch (SEN) specimens subjected to quasi-static loadings to investigate the effect of time-dependent behaviors on translaminar failure and strain energy release rate [4]. In other words, the fracture behavior and toughness depend on the contribution of both fiber and matrix nature to damage mechanisms. In addition, the translaminar crack growth resulting from an initial transverse notch is usually self-similar in quasi-isotropic brittle laminates [3-4]. In angle-ply ductile laminates, a self-similar crack growth may be expected in materials that have very strong matrix materials such as the matrix and the fiber/matrix interface are sufficiently strong to enable matrix cracking which results in the breakage of fibers due to stress concentration [4]. Thus, this idealization of a damage zone, which extends in a self-similar manner, allows a global analysis based on the evaluation of the total strain energy release-rate [8-9]. The experimental data used in the present work for comparison purposes with the numerical modelling results are drawn from previous works [10-11].

I.3 Modeling background

I.3.1 Numerical modelling of the strain energy release rate

The study of fracture mechanics in composite materials is not recent [12-16]. When it comes to investigate numerically the crack propagation in TP-based composites at high temperature as matrix toughness and viscous behavior are significantly enhanced, there is virtually no reference in the literature. It is known that the comprehension and the prediction of both initiation and propagation of primary damage in TP composites is highly related to the presence of singular stress and strain fields [17] responsible for the accommodation of

overstresses in high gradients zones (e.g. notches or holes). According to Vieille et al [18-19], the overstress accommodation is highly temperature-dependent in high-performance TP-based composites mainly under off axis loading. Hence, in order to account for the non-linear behavior (time-dependent and plastic behaviors) of TP-based laminates at high temperature, there is a need to develop a reliable model to capture their visco-elastic-plastic behaviors. The present work is based on a viscoelastic and viscoplastic model developed by Albouy et al. [20]. In the literature, many studies have been conducted to describe the time dependent behavior of Polymer Matrix Composites (PMCs). A comprehensive review is proposed in [20]. Most of the viscoelastic models presented in the literature such as Schapery's model, were initially elaborated for polymer materials and was later extended to composites [21]. At higher loading levels, the viscoplastic behavior becomes prominent and not surprisingly, the viscoelastic models lose their accuracy. Finally, in the vicinity of T_g, it turns out that most of the viscoelastic models are unable to precisely predict the viscous behaviors [22]. That's the reason why, a viscoelastic viscoplastic model has been developed for TP-based composites [20] and implemented into a Finite Element code Cast3m®.

The study and the comprehension of fracture mechanics in high performance TP composite require the development of numerical models able to evaluate the energy release rate and predict the initiation and crack growth process. The main purpose of the present work is then to determine the strain energy release rate G at crack initiation in high performance TP composite at $T > T_g$. Many numerical tools have been developed to provide the mechanical field state in the vicinity of the crack tip. Among them, the energy methods, based on unvarying integrals, appear to be efficient to evaluate the energy release rate in accordance with a thermodynamic approach [22-23]. Using such methods, it is possible to evaluate the fracture parameters far from the crack tip where the mechanical fields are largely disturbed by

a strong singularity. However, some of these tools are mathematically limited to simple or global fracture modes for isotropic or orthotropic media [23-24].

Using a contour integral related to energy in the vicinity of a crack, Rice proposed a method to solve 2D notch and crack problems in elastic-plastic materials [25]. The J-integral can be seen as the amplitude of the stress and strain singularity; the latter is often referred to as the HRR (Hutchinson-Rice-Rosengren) singularity [25-27] which is formally defined by the path-independent line integral:

$$J = \int_{\Gamma} \left(w(\varepsilon_{ij}).n_1 - \sigma_{ij}.n_j.\frac{\partial u_i}{\partial x} \right) d\Gamma \qquad (1)$$

Where Γ is an arbitrary curve encircling the crack tip oriented by its normal n_j, u_i designates the displacement component and w is the strain energy density defined as:

$$w = \int_0^{\varepsilon} \sigma_{ij} d\varepsilon_{ij} \qquad (2)$$

where σ_{ij} and ε_{ij} are the components of stress and strain, respectively.

However, the J-integral leads to difficulties in integrating fields at Gaussian points [28-30]. Alternatively, the G_θ-integral method, applicable to materials whose behavior can be elastic, viscoelastic and viscoplastic [29], provides a way to determine the strain energy release rate by using a surface integral. Initially developed by Destuynder et al. [31], the G_θ-integral is deduced from the J-Integral by operating, on the contour integral domain, a Gauss–Ostrogradsky transformation which changes the integration domain from a contour to a surface V. It is given by:

$$G_\theta = \int_V \left(-w.\theta_{k,k} + \sigma_{ij}.u_{i,k}.\theta_{k,j} \right) dV \qquad (3)$$

where V is a surface bounded by two contours.

$\vec{\theta}\begin{pmatrix}\theta_1\\\theta_2\end{pmatrix}$ is the virtual displacement field. It represents the virtual kinematics of the crack.

If J and G_θ integrals provide to determine an invariant leading at the mechanical state in the crack vicinity, they provide an overall computation regardless the modes of fracture (mode I or II, mixed modes). For this reason, these integrals are used only for pure opening or pure shear fracture modes [23-24]. In order to take into account the mixed mode separation, Noether proposed the conservative law method, based on an independent path integral [32]. This method is characterized by an expensive finite element discretization. Bui et al. have generalized the J-integral by proposing a separation between symmetric and antisymmetric displacement fields [33]. This method requires a symmetric mesh in the vicinity of the crack tip. Then, initially proposed by Chen et al. for elastic and isotropic materials [34], Moutou Pitti et al. have extended the M-integral to orthotropic materials based on virtual work principle [24]. Chen et al. have also introduced the M-integral adapted to isotropic and elastic material in order to separate mixed mode fracture [34]:

$$M = \frac{1}{2} \cdot \int_\Gamma \left(\sigma_{ij,1}^{(v)} \cdot u_i - \sigma_{ij}^{(u)} \cdot v_{i,1} \right) \cdot n_j d\Gamma \tag{4}$$

where $(\sigma_{ij}^{(u)}, u)$ and $(\sigma_{ij}^{(v)}, v)$ are the real and virtual stresses and displacement field respectively.

Then, this integral was modified from a curvilinear integral to a surface integral [24-44]. Thus, for plane problems, M_θ-integral takes the following form:

$$M_\theta = \frac{1}{2} \cdot \int_V \left(\sigma_{ij}^{(u)} \cdot v_{i,1} - \sigma_{ij,k}^{(v)} \cdot u_i \right) \cdot \theta_{k,j} dV \tag{5}$$

In the case of orthotropic materials and for each fracture mode, the virtual displacements fields are expressed as follows [33]:

$$v_1 = 2 \cdot K_1^{(\sigma)} \cdot \sqrt{\frac{r}{2 \cdot \pi}} \cdot \Re\left[\frac{1}{s_1 - s_2} \cdot \left(p_2 \cdot s_1 \cdot \sqrt{\rho_2} - p_1 \cdot s_2 \cdot \sqrt{\rho_1}\right)\right]$$

$$+2 \cdot K_2^{(\sigma)} \cdot \sqrt{\frac{r}{2 \cdot \pi}} \cdot \Re\left[\frac{1}{s_1 - s_2} \cdot \left(p_2 \cdot \sqrt{\rho_2} - p_1 \cdot \sqrt{\rho_1}\right)\right]$$

$$\tag{6}$$

$$v_2 = 2 \cdot K_1^{(\sigma)} \cdot \sqrt{\frac{r}{2 \cdot \pi}} \cdot \Re\left[\frac{1}{s_1 - s_2} \cdot \left(q_2 \cdot s_1 \cdot \sqrt{\rho_2} - q_1 \cdot s_2 \cdot \sqrt{\rho_1}\right)\right]$$

$$+2 \cdot K_2^{(\sigma)} \cdot \sqrt{\frac{r}{2 \cdot \pi}} \cdot \Re\left[\frac{1}{s_1 - s_2} \cdot \left(q_2 \cdot \sqrt{\rho_2} - q_1 \cdot \sqrt{\rho_1}\right)\right]$$

with $\rho_j = \cos(\theta) + i \cdot s_j \cdot \sin(\theta)$ avec $j \in \{1; 2\}$

and $p_j = S_{11} \cdot s_j^2 + S_{12}$ et $q_j = \frac{S_{22}}{s_j} + S_{12}$

s_j represent the roots of the following equation:

$$S_{11} \cdot s_\beta^4 + (2 \cdot S_{12} + S_{33}) \cdot s_\beta^2 + S_{22} = 0 \tag{7}$$

S_{11}, S_{12}, S_{22} and S_{33} are the components of the compliance tensor in an orthotropic body.

More recently, Moutou Pitti et al. have generalized this approach into viscoelastic behavior by combining the generalized Kelvin Voigt model and M_θ-integral in the case of an elastic body [23-24]. Eq. (5) becomes:

$$M\theta_v^{(k)} = \frac{1}{2} \cdot \int_V \left(\sigma_{ij}^{(k)}(u) \cdot u_i^{(k)} - \sigma_{ij,k}^{(v)}(v) \cdot v_{i,k}^{(k)}\right) \cdot \theta_{k,j} \, dV \tag{8}$$

with $k = (0, 1, \ldots, N)$, where N is the number of springs.

$\left(\sigma_{ij}^{(k)}(u), \, u_i^{(k)}\right)$ and $\left(\sigma_{ij,k}^{(v)}(v), \, v_i^{(k)}\right)$ are the real and virtual stresses and displacements in the kth spring.

This method is only applicable in the case of 2D configurations. In addition, although the viscoelastic behavior can be implicitly taken into account in the model through $M\theta_v$-integral, the mechanical fields are determined by considering an elastic behavior. Destunyder et al. have extended the G_θ method by introducing a vector field $\vec{\theta}$ allowing a virtual crown definition [31][36]. This crown should be far enough from the crack tip in order to obtain good approximation of the solution. The vector field $\vec{\theta}$ should verify the following properties:

- θ is parallel to the crack plan;

- θ is normal to the crack front;

- the support of θ is concentrated in the vicinity of the crack;

- $\|\theta\|$ is constant in a defined area around the crack tip

In 2D, two paths C_1 and C_2 can be considered around the crack tip. These paths divide the structure into three domains. For a given angle of inclination β, the vector field $\vec{\theta}$ can be expressed as follow [29]:

$$\begin{cases} \theta_1 = \left(1 - \dfrac{IM}{IJ}\right)\cos(\beta) \\ \theta_2 = \left(1 - \dfrac{IM}{IJ}\right)\sin(\beta) \end{cases}$$

where M is an integration point, I and J are the intersections between OM and C_1 and C_2 respectively.

Thus, θ is continuously differentiable and takes the following values in the three domains (see Figure 1):

- in C_{int}, $\|\theta\| = 1$;

- in C_{ext}, $\|\theta\| = 0$;

- in C_{cour}, $\|\theta\|$ varies continuously from 1 to 0.

I.3.2 Numerical modelling of time-dependent behaviors

The behavior of woven-ply thermoplastic laminates at temperature higher than their T_g was simulated using a time-dependent model. The purpose of this section was not to detail the model, but it is necessary to briefly recall the viscoelastic viscoplastic model constitutive laws. For more details, the reader can refer to [20]. In order to predict accurately the time dependent behavior carbon fibers woven-ply reinforced PolyPhenylene Sulphide (PPS) laminates at temperature higher than their T_g, a linear spectral viscoelastic model and a generalized Norton-type viscoplastic formulation developed for TS-based composites have been considered [20][37]. To a first approximation, the small strain formulation is used. Thus, under an incremental formalism, the total strain can be divided into three parts as follows:

$$\underline{\Delta\varepsilon} = \underline{\Delta\varepsilon}^e + \underline{\Delta\varepsilon}^{ve} + \Delta\underline{\varepsilon}^{vp} \tag{9}$$

where $\underline{\varepsilon}^e$ is the elastic strain, $\underline{\varepsilon}^{ve}$ is the viscoelastic one and $\underline{\varepsilon}^{vp}$ is the viscoplastic one.

Viscoelastic spectral linear model

In order to simulate the viscoelastic behavior of Polymer Matrix Composites (PMCs) at high temperature, a viscoelastic spectral linear model was chosen [20]. It consists in decomposing the viscoelastic strain rate $\underline{\dot{\varepsilon}}^{ve}$ into elementary mechanisms $\underline{\xi}_i$ which are associated with relaxation time spectrum such as:

$$\underline{\dot{\varepsilon}}^{ve} = \sum_{i=1}^{n_b} \underline{\xi}_i \tag{10}$$

where n_b is the total number of mechanisms, and the elementary viscous mechanisms $\underline{\xi}_i$ are defined by:

$$\dot{\underline{\xi}}_i = \frac{1}{\tau_i}\left(\mu_i \underline{\underline{S}}^{ve}\underline{\sigma} - \underline{\xi}_i\right) \tag{12}$$

where $\underline{\sigma}$ is the Cauchy stress tensor and $\underline{\underline{S}}^{ve}$ is the viscoelastic compliances tensor.

The viscoelastic formulation assumes a normal distribution of the relaxation mechanisms weights μ_i according to the relaxation time of the ith mechanism $n(i) = \log(\tau_i)$ where τ_i is the relaxation time:

$$\mu_i = \frac{1}{n_0\sqrt{\pi}} \times exp\left(-\left(\frac{n(i) - n_c}{n_0}\right)^2\right) \tag{11}$$

with $n_i = n_c + n_0 + (i - 1)\Delta$ is the ith relaxation mechanism and $\Delta = 2n_0/n_b - 1$ is the time interval separating two relaxation times. The spectrum is only described by two parameters: its standard deviation n_0 and its average value n_c.

In the case of woven ply, under the assumption of a purely elastic behavior in fibers directions (direction 1 and 2 in the case of a woven-ply lamina) and a plane stress state (thin laminated plate), $\underline{\underline{S}}^{ve}$ can be defined by:

$$\underline{\underline{S}}^{ve} = \begin{vmatrix} 0 & 0 & 0 & 0 & 0 & 0 \\ 0 & 0 & 0 & 0 & 0 & 0 \\ 0 & 0 & 0 & 0 & 0 & 0 \\ 0 & 0 & 0 & \beta_{44}/G_{12} & 0 & 0 \\ 0 & 0 & 0 & 0 & 0 & 0 \\ 0 & 0 & 0 & 0 & 0 & 0 \end{vmatrix} \tag{13}$$

where G_{12} is the shear modulus and β_{44} is a material viscosity parameter.

Generalized Norton-type viscoplastic model

In order to develop a satisfactory modelling at high stress levels, a generalized Norton-type viscoplastic model [37] is added to the viscoelastic model:

$$f_{vp}(\underline{\sigma} - \underline{X}) = \overline{(\underline{\sigma} - \underline{X})} - \tau_y(T) \tag{14}$$

with $\overline{(\underline{\sigma} - \underline{X})} = \sqrt{^T(\underline{\sigma} - \underline{X})\underline{\underline{M}}(\underline{\sigma} - \underline{X})}$

$\underline{\underline{M}}$ describes the viscoplastic flow anisotropy associated with the PPS matrix in shear loading:

$$\underline{\underline{M}} = \begin{vmatrix} 0 & 0 & 0 & 0 & 0 & 0 \\ 0 & 0 & 0 & 0 & 0 & 0 \\ 0 & 0 & 0 & 0 & 0 & 0 \\ 0 & 0 & 0 & 1 & 0 & 0 \\ 0 & 0 & 0 & 0 & 1 & 0 \\ 0 & 0 & 0 & 0 & 0 & 1 \end{vmatrix} \tag{15}$$

$\underline{X}$ is the thermodynamic force. In the case of a linear kinematics hardening, it is associated with $\underline{\alpha}$ such as $\underline{X} = \delta\underline{\alpha}$.

δ is a material parameter associated with the linear kinematic hardening.

The constitutive laws for the viscoplastic strain rate $\underline{\dot{\varepsilon}}^{vp}$ and the kinematic hardening rate $\underline{\dot{\alpha}}$ are derived from the thermodynamical potential f_{vp} such as:

$$\underline{\dot{\varepsilon}}^{vp} = K\langle f_{vp}\rangle^N \frac{\partial f_{vp}}{\partial \underline{\sigma}} \text{ and } \underline{\dot{\alpha}} = -K\langle f_{vp}\rangle^N \frac{\partial f_{vp}}{\partial \underline{X}} \tag{16}$$

where N represents the material rate sensitivity and K is a penalty coefficient. When $K \rightarrow \infty$, the classical time-independent plasticity expression is recovered. Therefore, the evolution laws can be expressed as follows:

$$\underline{\dot{\varepsilon}}^{vp} = \dot{\lambda}_{vp} \frac{\underline{\underline{M}}(\underline{\sigma} - \underline{X})}{\overline{(\underline{\sigma} - \underline{X})}} \text{ and } \underline{\dot{\alpha}} = \dot{\lambda}_{vp} \frac{\underline{\underline{M}}(\underline{\sigma} - \underline{X})}{\overline{(\underline{\sigma} - \underline{X})}} = \underline{\dot{\varepsilon}}^{vp} \tag{17}$$

where $\dot{\lambda}_{vp} = \sqrt{^T\underline{\dot{\varepsilon}}^{vp}\underline{\underline{M}}^{-1}\underline{\dot{\varepsilon}}^{vp}}$ is the Lagrange viscoplastic multiplier homogenous to a strain rate. Using a backward Euler method, the previous constitutive laws have been time-

discretized, and the resulting incremental laws have been implemented into the finite element code Cast3m® [20].

Parameters identification

It is noteworthy that the main advantage of the present modelling compared to other models found in the literature is the reduced number of parameters to identify. The parameters of the viscoelastic and viscoplastic constitutive laws are summarized in Table 1. The mechanical tests carried out to identify the parameters of the models are detailed in [20].

I.4 Objectives of the work

The G_θ-integral can be computed by means of the procedure G_THETA implemented in the finite element code Cast3m®. This procedure can deal with elastic, elasto-plastic and visco-plastic problems based on 2D, 3D or axisymmetric geometries, and can account for the behavior of homogenous, non-homogeneous or composite materials. It can also be used to separate the mixed modes for homogenous and isotropic materials. However, this procedure is complicated and it's very difficult to adapt it to external constitutive laws. In addition, by analyzing the analytical form of G_θ-integral, one can notice that it is expressed in term of displacement, strain and stress mechanical fields. In this context, the idea was to apply directly the G_θ integral form based on the CH_THETA procedure implemented into the finite element code Cast3m® in order to create a θ field. In order to accurately evaluate the G_θ-integral using G_θ method, it is required to predict accurate local mechanical fields in the vicinity of the crack tip by means of optimized meshing. This can be achieved by using the viscoelastic viscoplastic model constitutive laws implemented in Cast3M [20].

Thus, the mode I strain energy release rate was evaluated by using G_θ-integral method based on the mechanical fields at the crowns surrounding the crack tip. The independence path integral was examined by representing the evolution of the strain energy release rate versus each crown in laminates characterized by viscoelastic viscoplastic behaviours at high temperature. Then, the strain energy release rate was plotted as a function of the applied load and crack growth. The obtained results were compared to experimental ones. It's worth precising that the purpose of the present work is not to simulate the crack growth under mechanical loading but to evaluate the capability of this method to determine the mode I strain energy release rate for different loading levels at crack initiation.

II. Results and discussion

II. 1 Meshing strategies

In order to test the capability of the numerical model to predict the response (overstress and overstrain profiles) of high-gradient structures [38], simulations have been carried out on Single Edge Notched (SEN) specimens, characterized by a ratio *a/w*=0.3. For symmetry reasons, only a half of the plate is modelled. Although reduction in the mesh size leads to more accurate FE solution, the finer mesh refinement requires more computation time. That is the reason why, it is necessary to find a compromise between accuracy requirements and computation time [39]. To this end, three-node triangular elements (Discrete Kirchhoff Triangles - DKT) have been used to mesh the crack tip with higher mesh density and two different types of meshing (radiant and concentric – see Figure 2) around the crack tip were tested, allowing us to generate crowns around the crack tip. Indeed, crowns, whose boundaries coincide with elements sides, have a crucial role when computing the strain energy release rate by means of the G_θ method. In addition, the numerical integration is performed at Gauss integration points of elements belonging to the crown, giving therefore more accurate results.

The numerical overstress and overstrain profiles was validated through the comparison with theoretical stress fields and longitudinal overstrain fields obtained from experimental full-field measurements (by Digital Image Correlation technique). The selected meshing type was then used to simulate the numerical overstrain and overstress profiles for AP laminates [39]. One of the most important criteria for selecting an efficient mesh is its ability to generate accurate overstress and overstrain fields in high gradient zones. Indeed, the issue of stress concentration in composite materials design has always been of great interest to researchers [40-42], and many studies have been conducted to investigate the effect of stress concentration zones (notches, holes…) on the mechanical properties of composites [43].

II. 2 Numerical modelling of the strain energy release rate

The strain energy release rate was computed by means of the numerical model in the case of laminates with two different stacking sequences: a Quasi-Isotropic (QI) sequence characterized by a fibre-dominated behaviour and an Angle-Ply (AP) sequence whose behaviour is matrix-dominated. It is expected that the PPS matrix viscoelastic-viscoplastic behavior has significant influence on the values of the strain energy release rate.

First of all, from the macroscopic standpoint, the proposed model predicts suitably the tensile mechanical response of notched specimens consisting of angle-ply and quasi-isotropic stacking sequences (see Figure 3). In QI specimens, a radiant meshing appears to be slightly more accurate than the concentric meshing. From the G_θ method introduced in section I.3, it is possible to estimate the strain energy release rate in AP and QI laminates. For the two stacking sequences, two ratios *a/w=0.2* and a/w=0.3 were studied. These ratios were chosen to obtain a strain energy release rate which is stabilized far from both the crack tip and the specimen edge. In fact, it is necessary to choose an integration crown in such a way as to validate the path independence domain. Figures 4-7 show the evolution of the strain energy

release rate according to the ith integration crown in QI and AP laminates. It appears that G_θ highly depends on the integration crown. In both cases, G_θ increases gradually until a constant value is reached. It's the high singularity of the mechanical fields which disturbs the field integration around the crack tip. Based on Eq. (5) and G_θ-method detailed in section I.3, the strain energy release rate was determined for different testing conditions.

The behavior of QI laminates is almost elastic brittle and it's characterized by rapid crack extension until brittle failure. However, the material exhibits a stable crack growth before crack initiation. Thus, it is important to consider the gradual propagation of the crack in the model. Figure 8 represents a comparison between numerical and experimental evolution of the strain energy release rate as a function of the applied load by considering computations with gradual crack growth (referred to as artificial propagation in Fig. 8). For *a/w=0.2*, the numerical results are satisfactory by considering the artificial propagation, though the simulation with *a/w=0.3* shows some discrepancy between experimental and numerical results. Similarly for G-R curves in the case of QI laminates (see Figure 9).

In AP specimens with small ratios *a/w* (e.g. *a/w=0.2*), crack tip blunting is observed before reaching the critical strain energy release rate without important crack propagation [7], hence justifying that only crack opening is taken into account. Figure 10a represents the evolution of the strain energy release rate as a function of the applied load before the critical load. For *a/w=0.3*, the numerical result seems to be in accordance with the experimental results. However, a discrepancy is observed in the case of *a/w=0.2*, as the model doesn't take into account crack tip blunting coming along with large fiber rotation and displacement near the crack tip [39] to accurately simulate the J-R curves (see Figure 10b). In addition, along with the instability of the crack propagation, it appears essential to use an automatic remesher which takes into account the crack propagation at each time step as well as its direction.

Finally, G_θ-method provides an overall computation of the strain energy release rate in mode I; and cannot give an accurate approximation of the strain energy release rate in mode II as AP laminates are characterized by a mixed failure mode [3].

III. Conclusion

Within the framework of fracture mechanics, the determination of G-R (brittle fracture) and J-R curves (ductile fracture) is utmost important to quantify fracture in terms of energy required to grow a crack in laminates with different lay-ups. Thus, the purpose of the present work was to apply the G_θ-integral in the case of C/PPS laminates characterized by a locally more or less significant time-dependent behavior at T>Tg in order to determine the mode I strain energy release rate (associated with the fracture toughness) at crack initiation. Depending on the stacking sequence, the highly viscous behavior of TP-based laminates at high temperature contributes to the increase in the fracture energy. By means of a time-dependent model implemented in the finite element code Cast3m and a meshing optimization, accurate mechanical fields have been simulated in the vicinity of the crack tip. A radiant mesh was selected to compute the mode I strain energy release rate by applying the G_θ method to AP and QI laminates with different ratios a/w. The R-curves have been derived from the computation of the strain energy release rate and the corresponding crack length. Ultimately, it is possible to build R-curves based on these numerical evaluations of fracture toughness and to compare these curves to the ones obtained from experiments.

Due to different phenomena (such as damage and crack instability) which are not taken into account by the model, a few discrepancies between experimental and numerical can be observed after crack initiation. The obtained results are highly sensitive to crack stability as, once the crack is initiated, it starts propagating in instable manner. To control the stability of the crack, compact tension specimens could prove to be relevant as the crack growth is

inherently stable in such specimens. In addition, a remeshing technique will be considered to account for translaminar crack propagation, and to allow the model to improve its predictive capability.

References

[1] JK. Wells, PWR. Beaumont. Crack-tip energy absorption processes in fibre composites. Journal of Materials Science, 20 (1985) 2735-2749.

[2] JK. Wells, PWR. Beaumont. The prediction of R-curves and notched tensile strength for composite laminates. Journal of Materials Science, 22 (1987) 1457-14.

[3] B. Vieille, M. Chabchoub, D. Bouscarrat, C. Gautrelet. Influence of matrix ductility and toughness on strain energy release rate and failure behavior of woven-ply reinforced thermoplastic structures at high temperature. Compos Part B, 132 (2018) 125-140.

[4] B. Vieille, M. Chabchoub, D. Bouscarrat, C. Gautrelet. A fracture mechanics approach using Acoustic Emission technique to investigate damage evolution in woven-ply thermoplastic structures at temperatures higher than glass transition temperature. Compos Part B, 116 (2017) 340-351.

[5] B. Lauke, W. Pompe. Fracture toughness of short-fibre reinforced thermoplastics. Composites Science and Technology, 26 (1) (1986) 37-57.

[6] K-Y. Kim, K-M Phoa. Interlaminar fracture toughness of CF/PEI and GF/PEI composites at elevated temperatures. Applied Composite Materials, 11 (2004) 173–190,.

[7] M. Chabchoub, B. Vieille, M. Beyaoui, M. Taktak, M. Haddar, L. Taleb. Determination of J-R curves by load separation criterion in highly ductile TP-based composites under high temperature conditions. Composite Structures, 182 (2017) 391–401.

[8] PWR. Beaumont. Physical modelling of damage development in structural composite materials under stress. In: Harris B, editor. Fatigue in composites: science and technology of

the fatigue response of fiber-reinforced plastics. Chapter 13. Cambridge: Woodhead Publishing Ltd.; 2003. p. 365-412.

[9] JM. Whitney, RJ. Nuismer. Stress fracture criteria for laminated composites containing stress concentrations. Journal of Composite Materials, 8(3) (1994) 253-265.

[10] B. Vieille, M. Chabchoub, D. Bouscarrat, C. Gautrelet. A fracture mechanics approach using Acoustic Emission Technique to investigate damage evolution in woven-ply thermoplastic structures at temperatures higher than glass transition temperature. Composites Part B 116 (2017) 340-351.

[11] B. Vieille, M. Chabchoub, C. Gautrelet. Influence of matrix ductility and toughness on strain energy release rate and failure behavior of woven-ply reinforced thermoplastic structures at high temperature. Composites Part B 132 (2018) 125-140.

[12] M. Valentini, S.K. Sekov, D. Bigoni, A.B. Movcha. Crack propagation in a Brittle elastic material with defects. Journal of Applied Mechanics, 66 (1) (1999) 79-86.

[13] H.M. Belmonte, SL. Ogin, PA. Smith, R. Lewin. A physically-based model for the notched strength of woven quasi-isotropic CFRP laminates. Composites Part A, 35 (7–8) (2004) 763-778.

[14] S.T. Pinho, P. Robinson, L. Iannucci. Fracture toughness of the tensile and compressive fibre failure modes in laminated composites. Composites Sciences and Technology, 66 (2006) 2069-2079.

[15] M. Shameli, N. Choupani. Fracture criterion of woven Glass-Epoxy Composite using a new modified mixed-mode loading fixture. International Journal of Applied Mechanics, 08(02) (2016) 1650015.

[16] M. Fan, D.K. Yi, Z.M. Xiao. Elastic-plastic fracture behavior analysis on a Griffith crack in the cylindrical three-phase composites with generalized Irwin model. International Journal of Applied Mechanics, 06(04) (2014) 1450045.

[17] A. Pupurs. Micro-crack Initiation and Propagation in Fiber Reinforced Composites. Lulea, Sweden: Ph.D. thesis, Department of Engineering Sciences and Mathematics, Lulea University of Technology, (2012).

[18] B. Vieille, J. Aucher, L. Taleb. Overstress accommodation in notched woven-ply thermoplastic laminates at high-temperature: numerical modeling and validation by digital image correlation. Composites Part B, 45(1) (2012) 290-302.

[19] B. Vieille, J. Aucher, L. Taleb. About the influence of temperature and matrix ductility on the behaviour of carbon woven-ply PPS or epoxy laminates: notched and unnotched laminates. Comp Sc and Tech, 71 (2011) 998-1007.

[20] W. Albouy, B. Vieille, L. Taleb. Experimental and numerical investigations on the time-dependent behavior of woven-ply PPS thermoplastic laminates at temperatures higher than glass transition temperature. Composites Part A, 49 (2013) 165-178.

[21] B. Bonnet, A. Thionnet, P. Carrier, J. Renard. Matériaux composites soumis à de grandes vitesses de sollicitation. Analyse expérimentale et modélisation, Revue des composites et des matériaux avancés, 14(1) (2004) 89-106.

[22] M.S. Al-Haik, M.Y Hussaini, H. Garmestani. Prediction of nonlinear viscoelastic behavior of polymeric composites using an artificial neural network. International Journal of Plasticity, 22(7) (2006) 1367-1392.

[23] R. Moutou Pitti, F. Dubois, M. Taazount. Finite element analysis and Fracture in viscoelastic materials by Mv integral-Part I: crack initiation. Finite Element Analysis, David Moratal (Ed.), (2010) ISBN: 978-953-307-123-7, InTech Editions.

[24] R. Moutou Pitti, F. Dubois, C. Petit, N. Sauvat. Mixed mode fracture separation in viscoelastic orthotropic media: numerical and analytical approach by the $M_{\theta v}$-integral. International Journal of Fracture, 145(3) (2007) 181-19.

[25] J.R. Rice. A path independent integral and the approximate analysis of strain concentration by notches and cracks. Journal of Applied Mechanics, 35 (1968) 379-386.

[26] J.R. Rice, G.F. Rosengren. Plane strain deformation near a crack tip in a power-law hardening material. Journal of the Mechanics and Physics of Solids, 16 (1968) 1-12.

[27] J.W. Hutchinson. Plastic stress and strain fields at a crack tip. Journal of the Mechanics and Physics of Solids, 16 (1968) 13-31.

[28] F. Dubois, C. Petit. Modelling of the crack growth initiation in viscoelastic media by the G_θ-integral. Engineering Fracture Mechanics, 72 (2005) 2821- 2836.

[29] F. Dubois, C. Chazal, C. Petit. A finite element analysis of creep-crack growth in viscoelastic media. Mechanics of Time-Dependent Materials, 2 (1999) 186-269.

[30] P.O. Bouchard. Contribution à la modélisation numérique en mécanique de la rupture et structures multi matériaux. Paris, France: Ph.D. thesis, Materials Science and Engineering, Ecole Nationale Supérieure des Mines (2000).

[31] P. Destuynder, M. Djaoua. Sur une interprétation mathématique de l'intégrale de Rice en théorie de la rupture fragile. Mathematical Methods in the Applied Sciences, 3(1981) 70-87.

[32] E. Noether. Invariant variations problem. Transport Theory and Statistical Physics, 1(3) (1971) 183-207.

[33] H.D. Bui, J.M. Proix. Découplage des modes mixtes de rupture en thermo-élasticité par des intégrales indépendantes du contour. Actes du Troisième Colloque Tendances Actuelles en Calcul de Structure, Bastia, (1985), pp 631–643.

[34] F. Chen, R. Shield. Conservation laws in elasticity of the J-integral type. Journal of Applied Mechanics and Physics, 28(1) (1977) 1-22.

[35] G.C. Sih. Strain-energy-density factor applied to mixed mode crack problems, International Journal of Fracture, 10(3) (1974) 305–321.

[36] P. Destuynder, P.E.M. Djaoua, L. Chesnay, J.C. Nedelec. Sur une interprétation mathématique de l'intégrale de Rice en théorie de la rupture fragile. Mathematical Methods in the Applied Sciences, 3(1) (1981) 70-87.

[37] M.L. Boubakar, L. Vang, F. Trivaudey, D. Perreux. A meso-macro finite element modelling of laminate structures: part II: time-dependent behaviour. Composite Structures, 60(3) (2003) 275-305.

[38] B. Vieille, W. Albouy, L. Taleb. Viscoelastic viscoplastic model for aeronautical thermoplastic laminates at high temperature: Validation on high stress gradient structures. Composites Part B, 90 (2016) 278-286.

[39] M. Chabchoub, B. Vieille, M. Beyaoui, M. Taktak, M. Haddar, L. Taleb. Investigations on crack propagation and strain energy release rate in notched woven-ply thermoplastic laminates at high-temperature, Int. Journal of Applied Mechanics, 8(6) (2016) 1–19.

[40] S.C. Tan. Finite-width correction factors for anisotropic plate containing a central opening. Journal of Composite Materials, 22 (1988) 1080-1097.

[41] S.C. Tan. Stress concentration in laminated composites (éd. Lancaster, Pa.: Technomic Pub. Co.), 1994.

[42] Z.M. Huang, L.M. Xin., Stress concentration factor in matrix of a composite subjected to transverse compression. International Journal of Applied Mechanics, 08(03) (2015) 1650034.

[43] C.J. Liu, A.H. Nijhof, L.J. Ernst. A new ultimate strength model of notched composite laminates including the effects of matrix. Journal of Composite Materials, 44(2010) 1335–1349.

[44] H. Riahi H, R. Moutou Pitti, F. Dubois, A. Chateauneuf. Mixed-mode fracture analysis combining mechanical, thermal and hydrological effects in an isotropic and orthotropic material by means of invariant integrals. Theoretical and Applied Fracture Mechanics, 85 (2016) 424-434.

Figure captions

Figure 1 - *Integration domain used for G$_\theta$ method*

Figure 2 - *Meshing of the notched specimens with zoom on the crack-tip area: (a) Concentric mesh (3933 elements) – (b) Radiant mesh (2061 elements)*

Figure 3 - *Monotonic tensile tests on notched C/PPS laminates - experience vs numerical modelling: (a) AP – (b) QI*

Figure 4 - *Path independence domain for a/w=0.2 in notched QI laminates: (a) Evolution of the strain energy release rate according to each crown – (b) θ field in the 28th crown*

Figure 5 - *Path independence domain for a/w=0.3 in notched QI laminates: (a) Evolution of the strain energy release rate according to each crown – (b)θ field in the 26th crown*

Figure 6 - *Path independence domain for a/w=0.3 in notched AP laminates: (a) Evolution of the strain energy release rate according to each crown – (b) θ field in the 12th crown*

Figure 7 - *Path independence domain for a/w=0.2 in notched AP laminates: (a) Evolution of the strain energy release rate according to each crown – (b)θ field in the 30th crown*

Figure 8 - *Comparison between numerical and experimental strain energy release rate as a function of the applied load in notched QI laminates: (a) a/w=0.2 and (b) a/w=0.3*

Figure 9 - *Comparison between numerical and experimental G-R curves in notched QI laminates: (a) a/w=0.3 – (b) a/w=0.2*

Figure 10 - *Comparison between numerical and experimental results in notched AP laminates: (a) evolution of the strain energy release rate as a function of the applied load for a/w=0.2 and a/w=0.3 – (b) J-R curves in the case a/w=0.2*

(a)

(b)

F_{imp}

F_{imp}

X

Y

X

Y
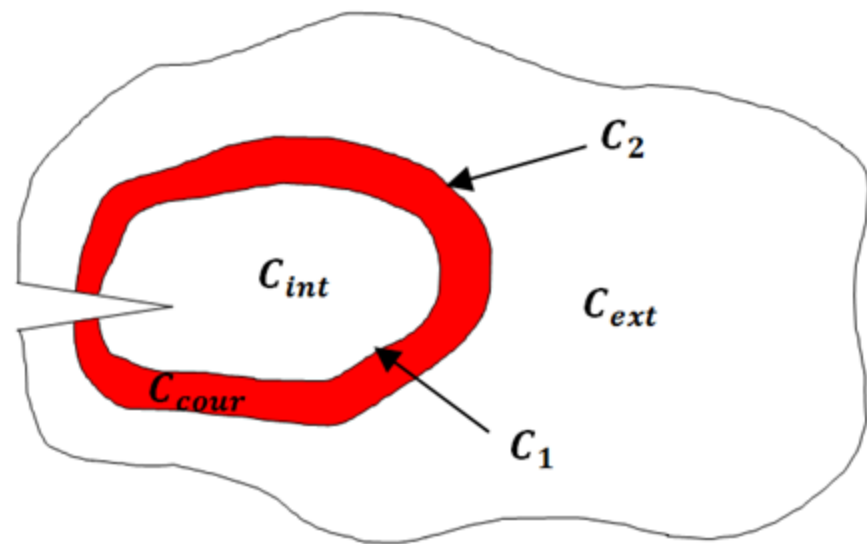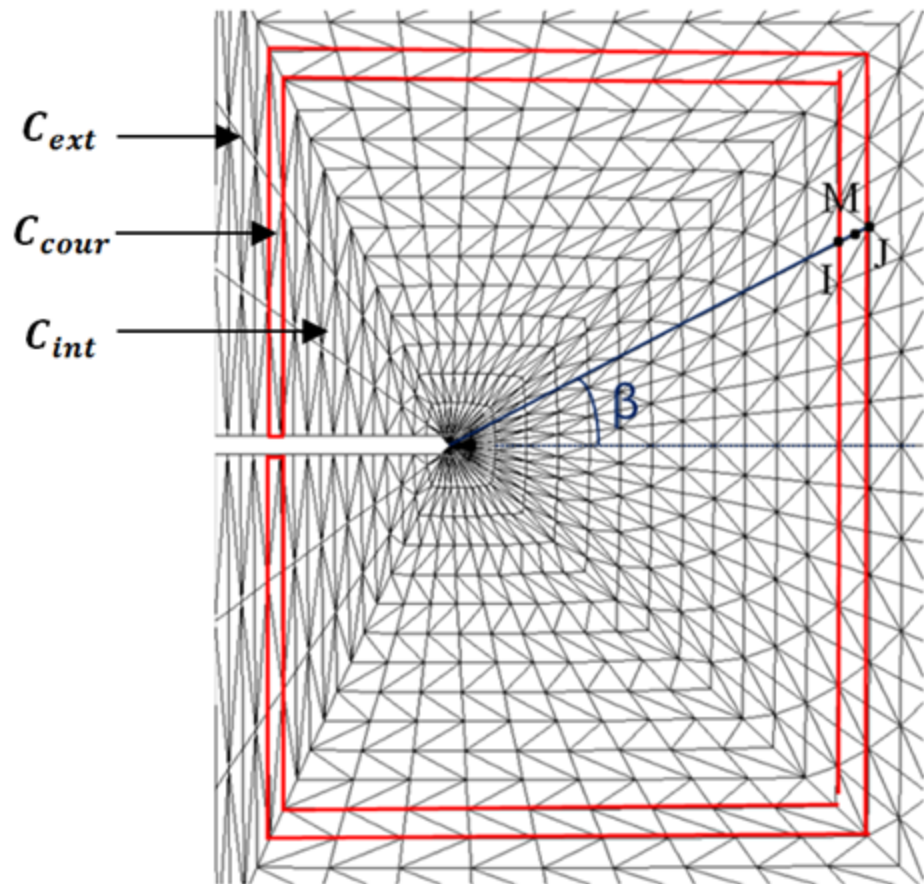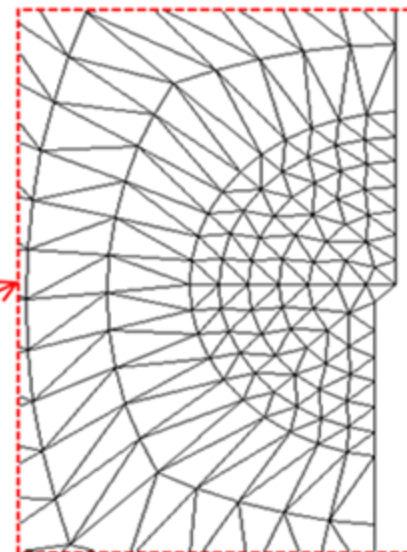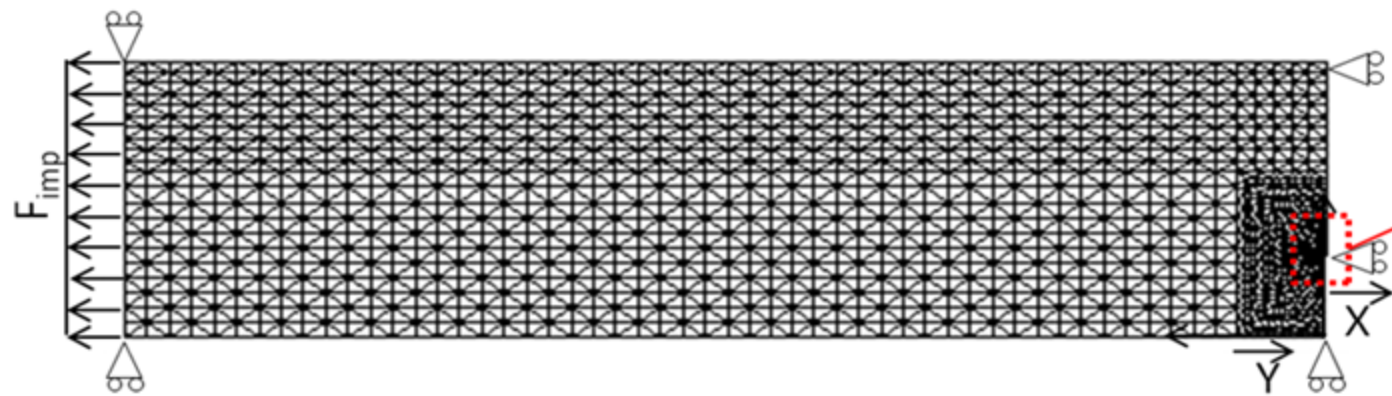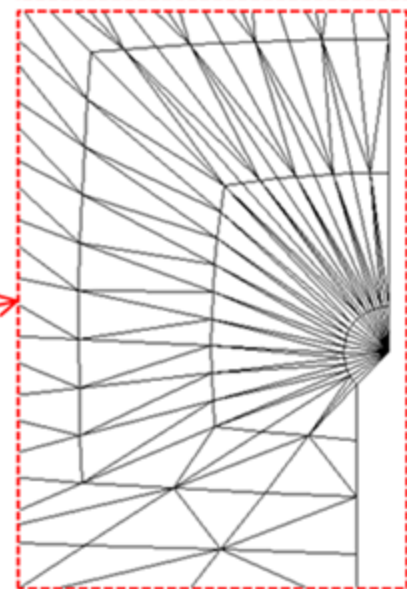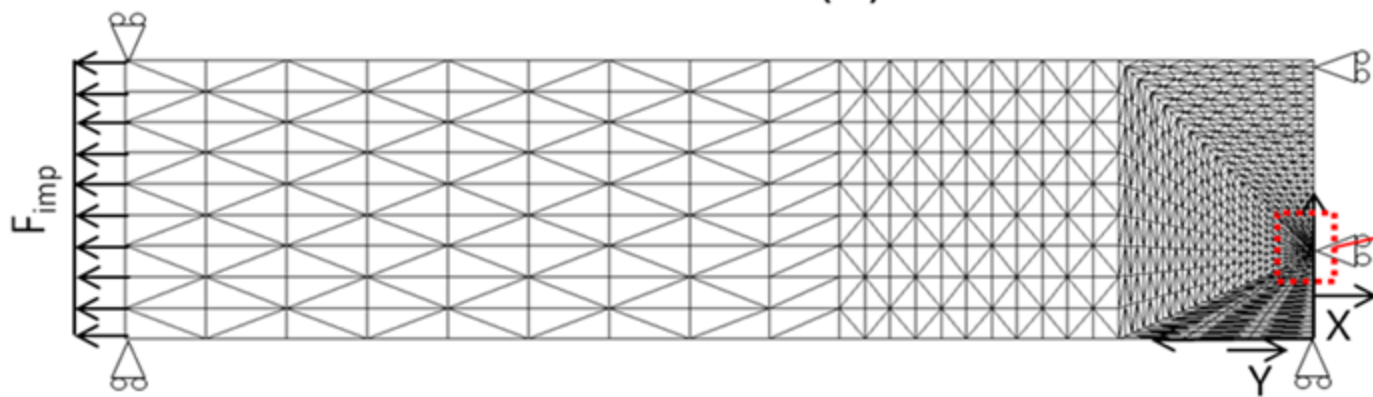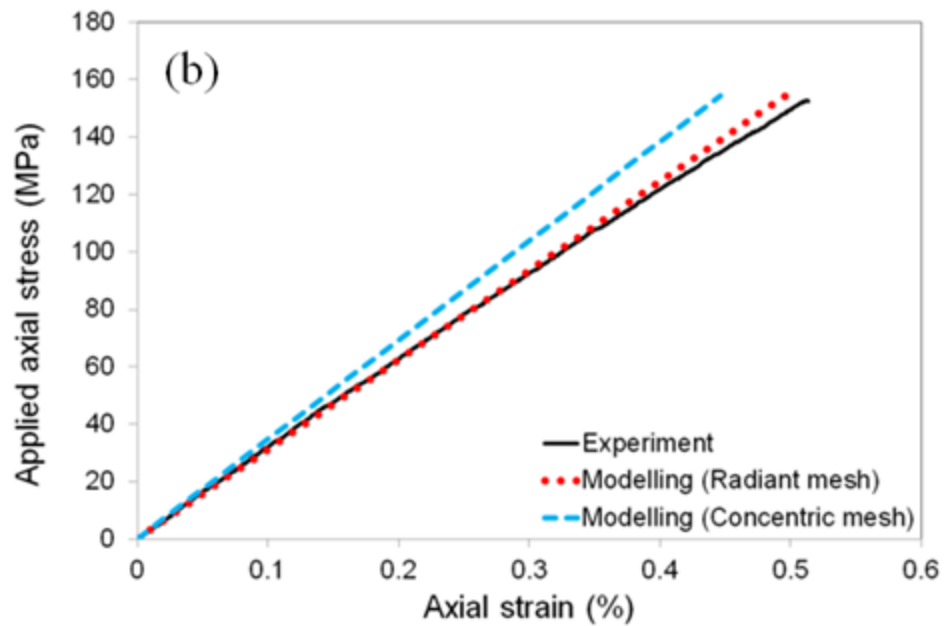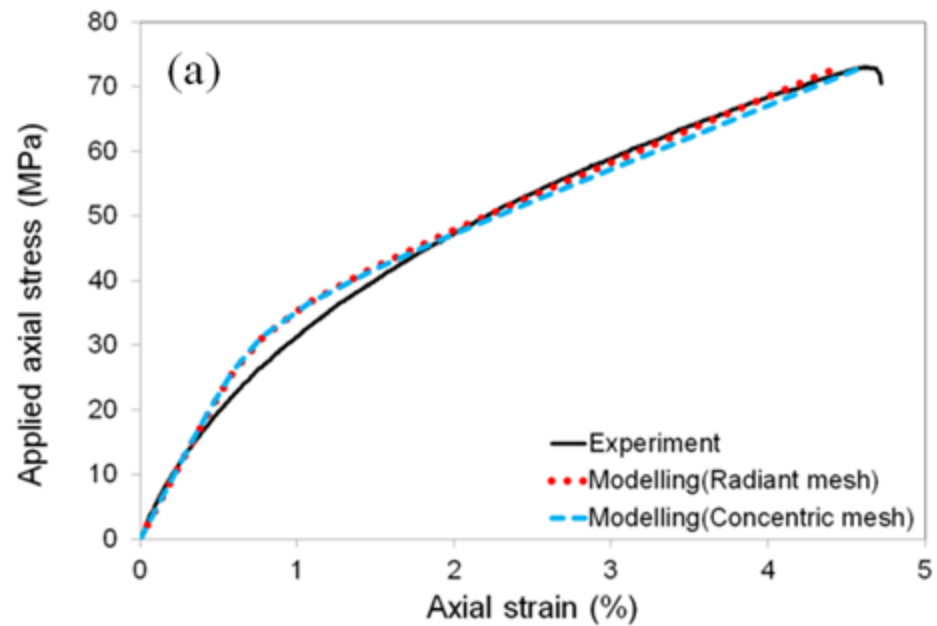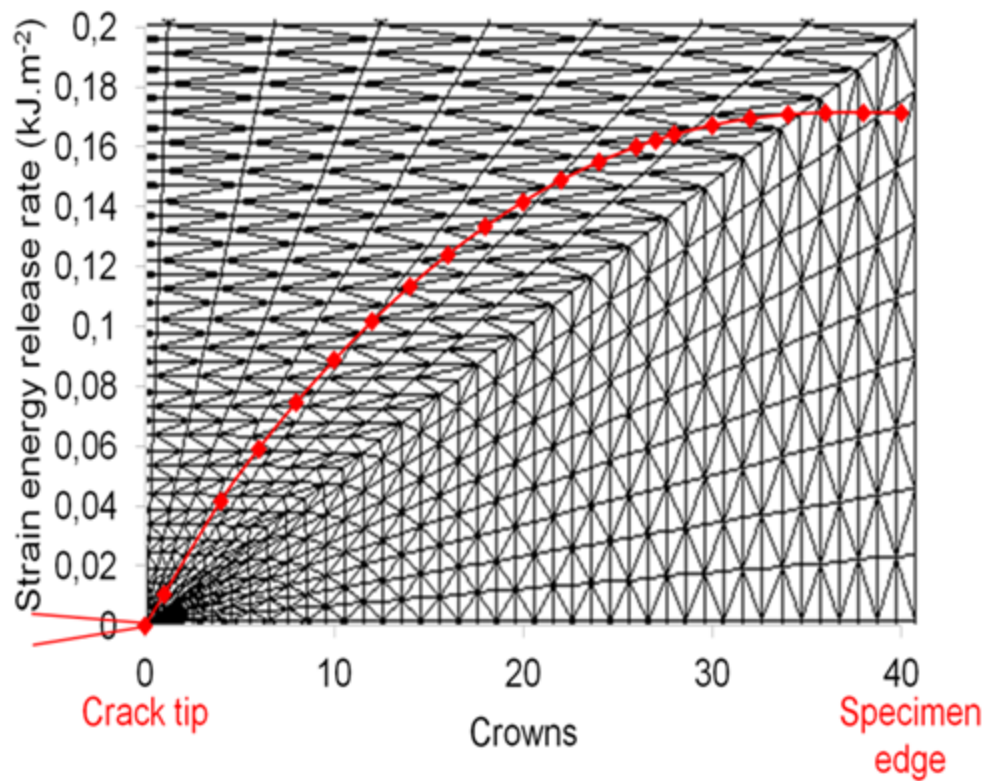
(a)   (b)
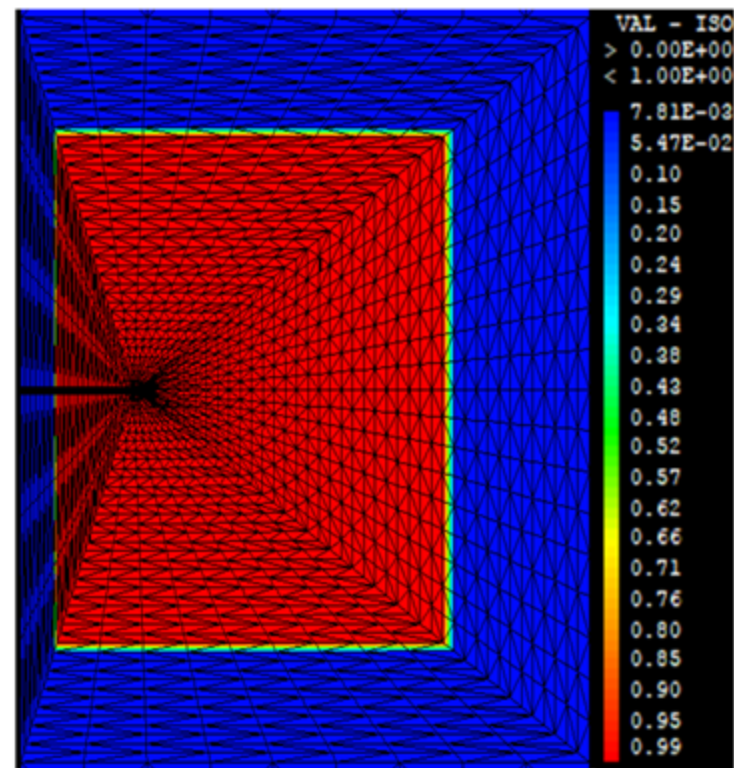
(a)
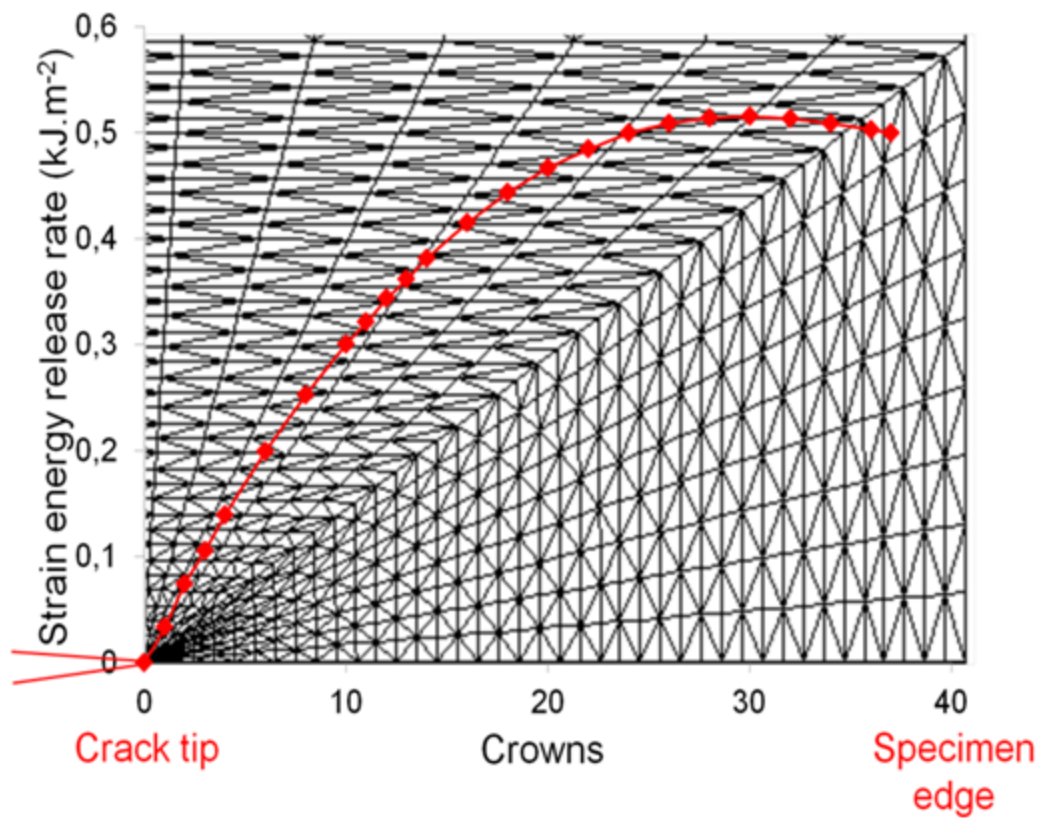
(b)
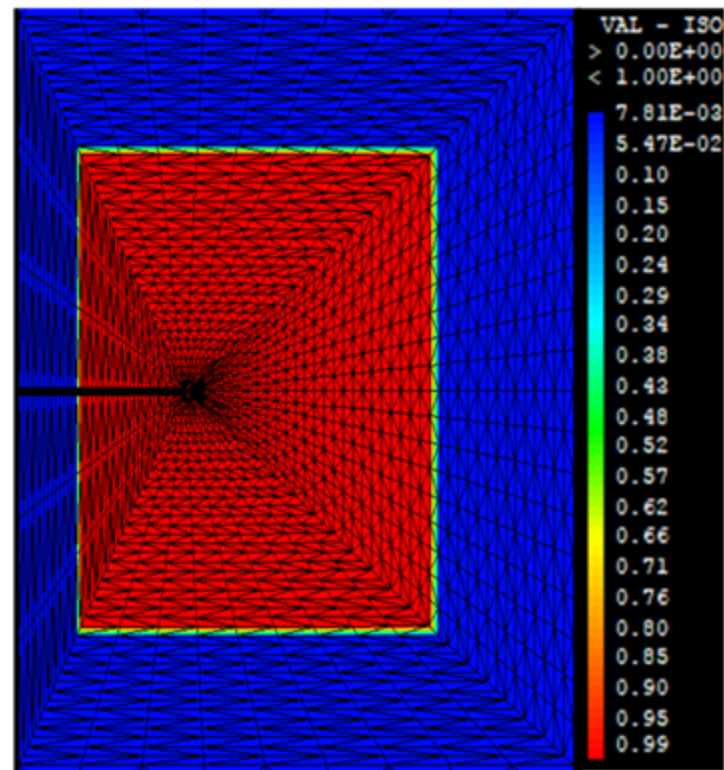
(a)
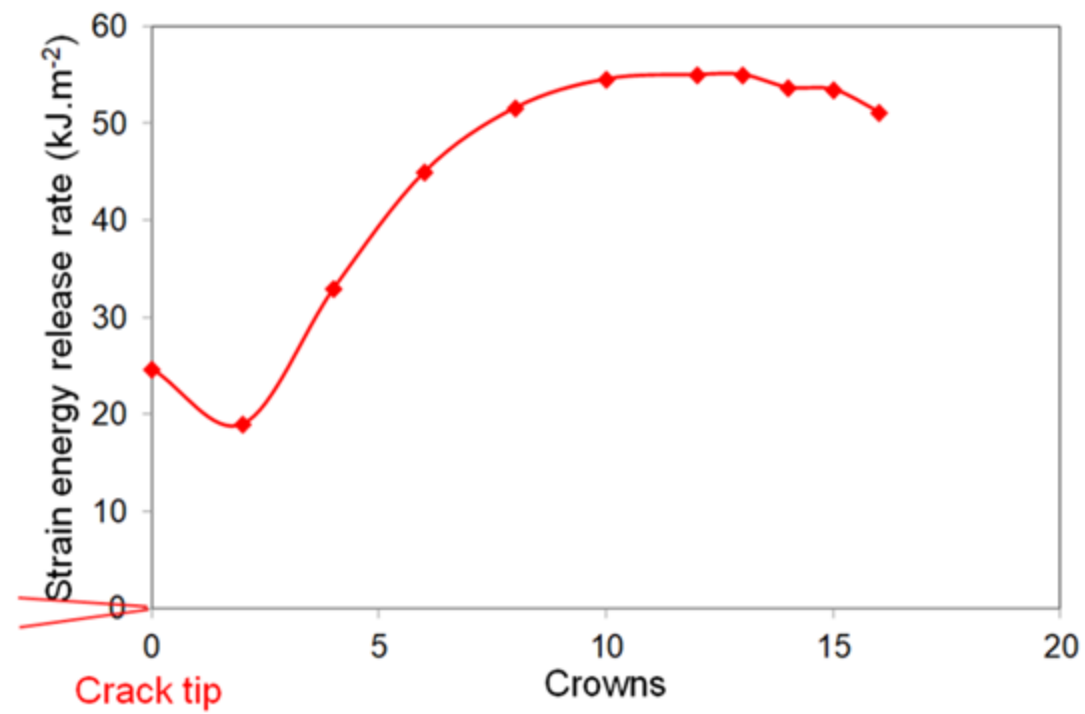
(b)
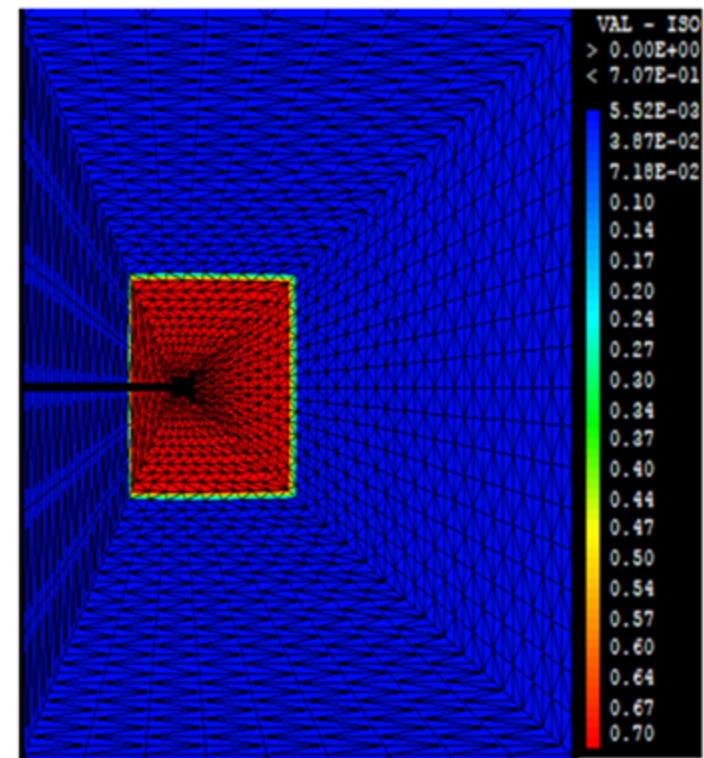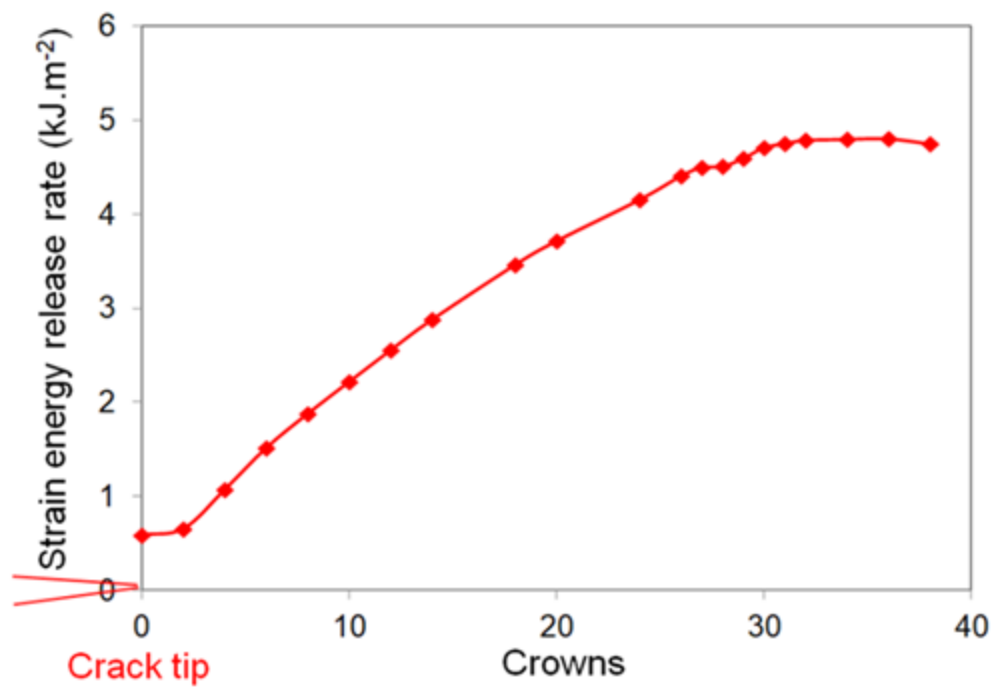
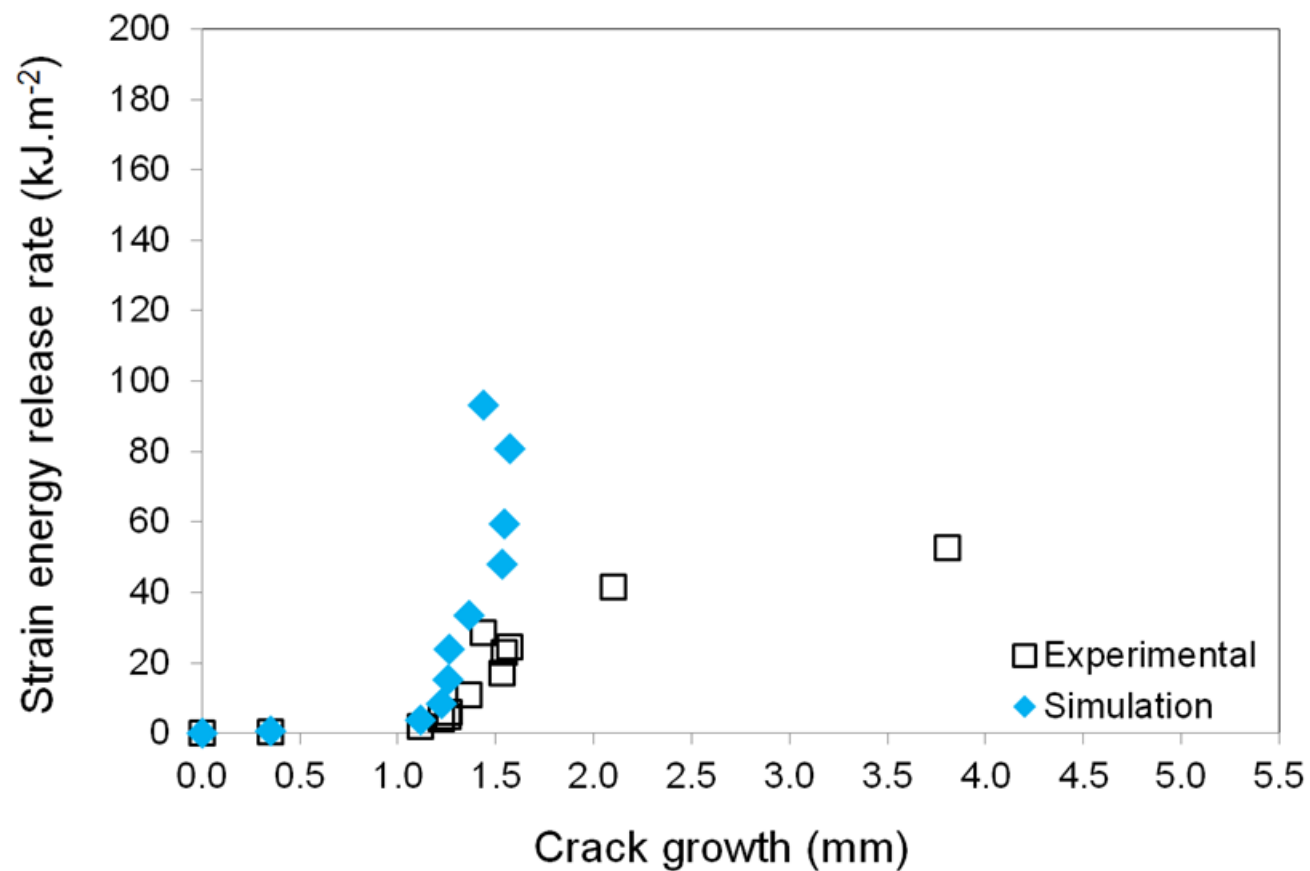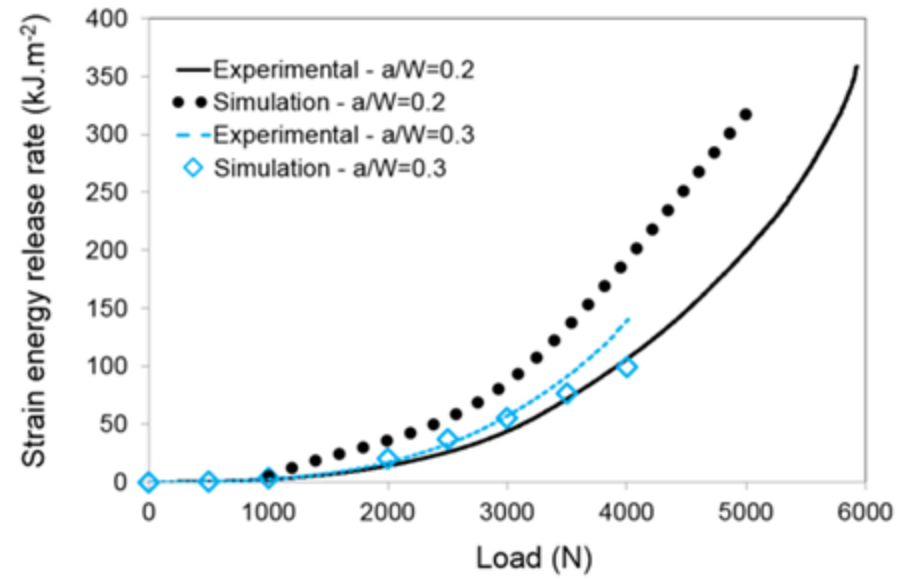(a)   (b)
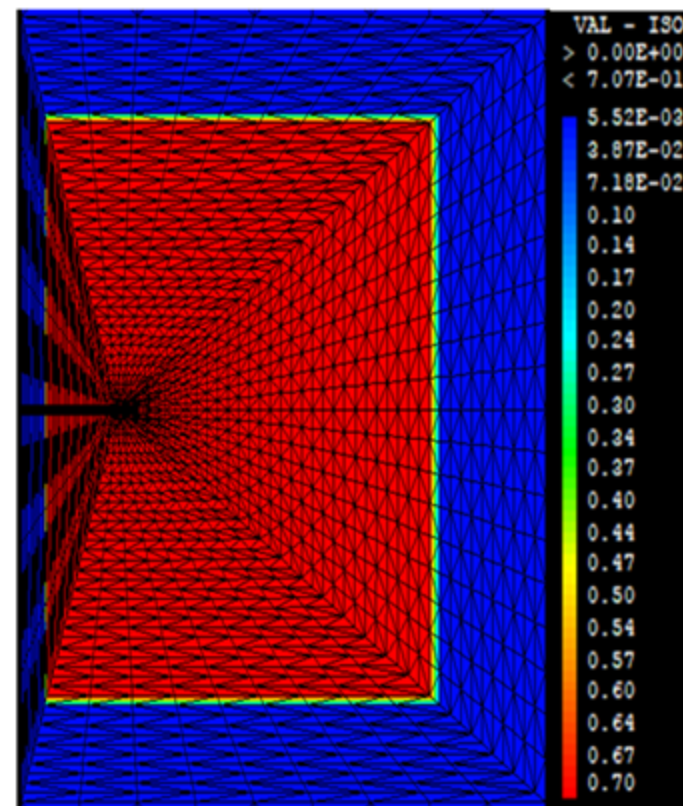
(a)
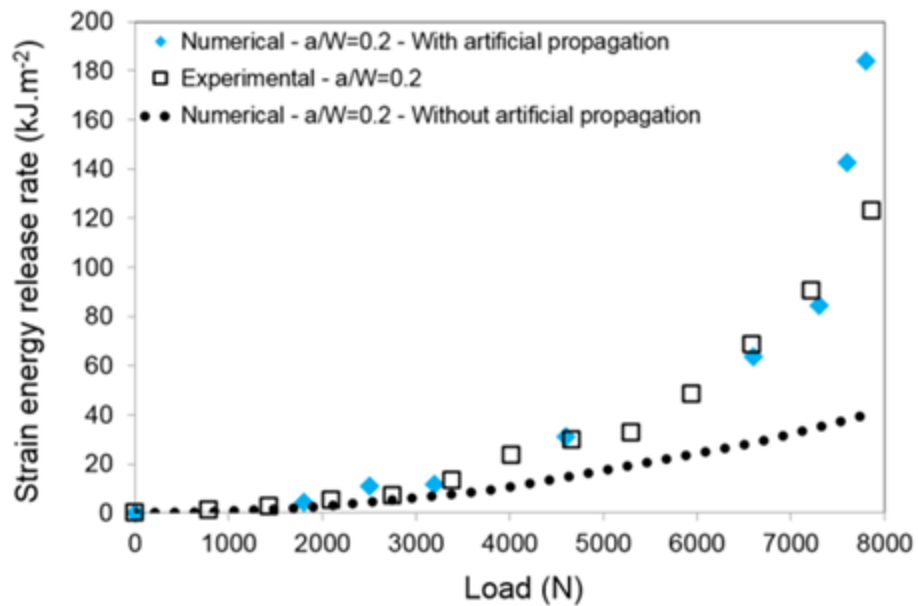
(b)
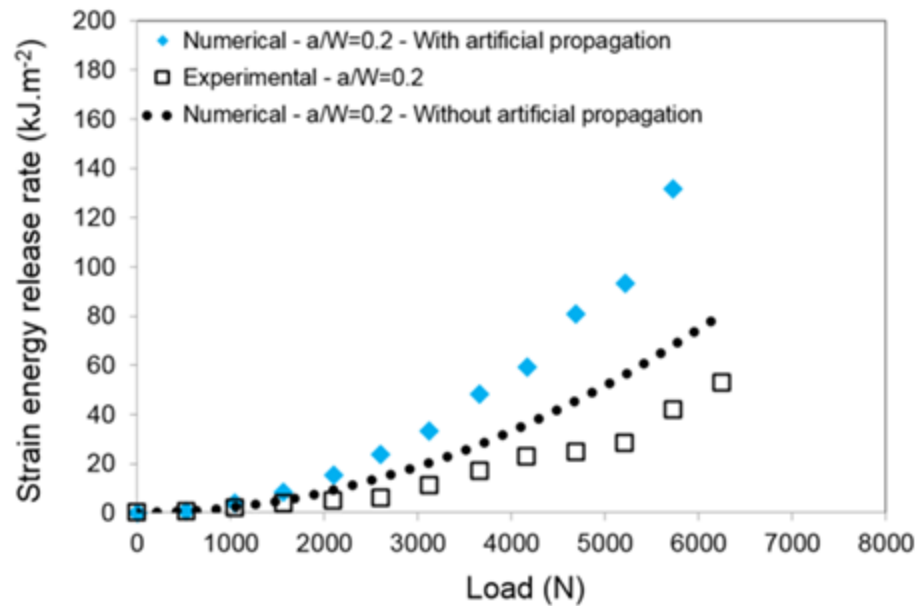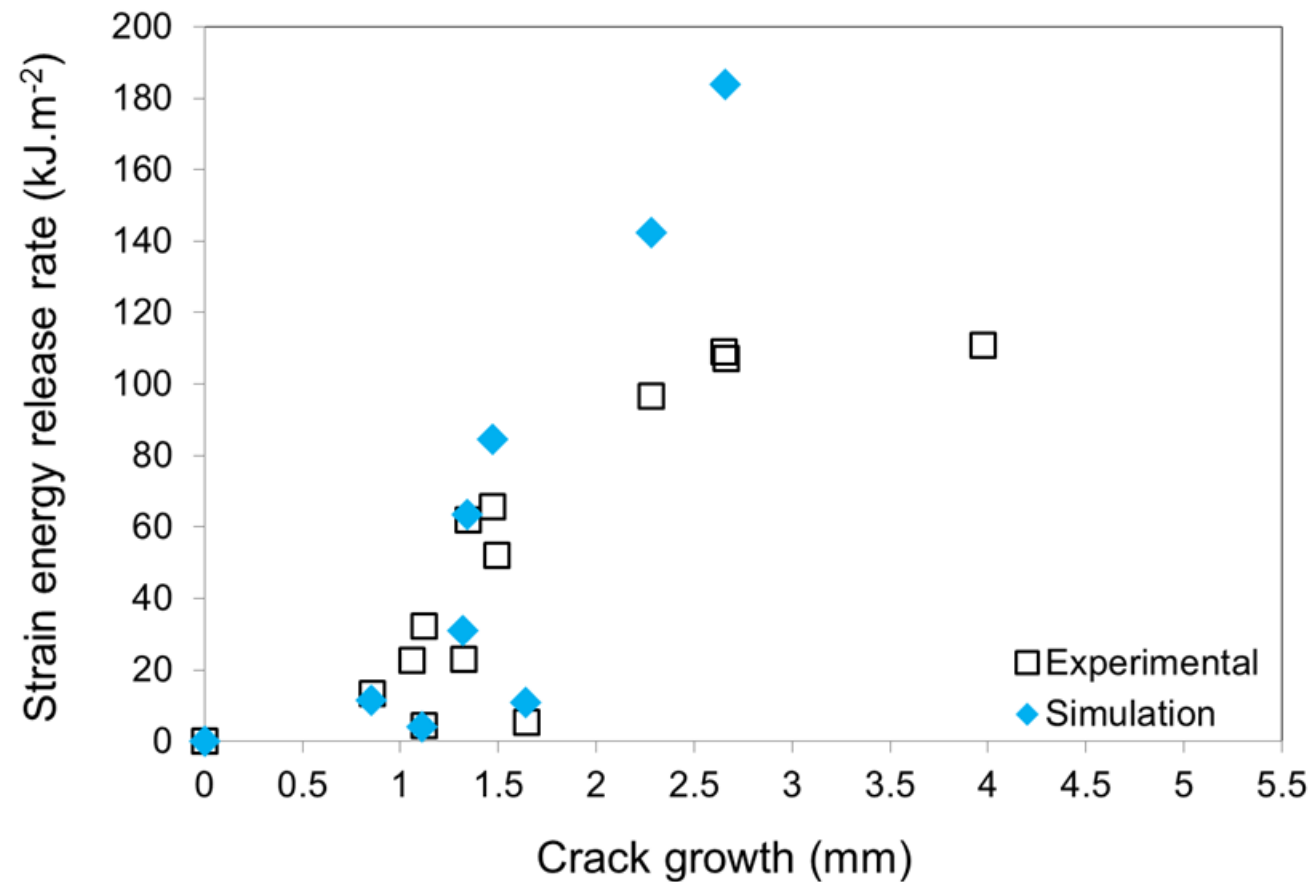
(a)   (b)

(a)

(b)
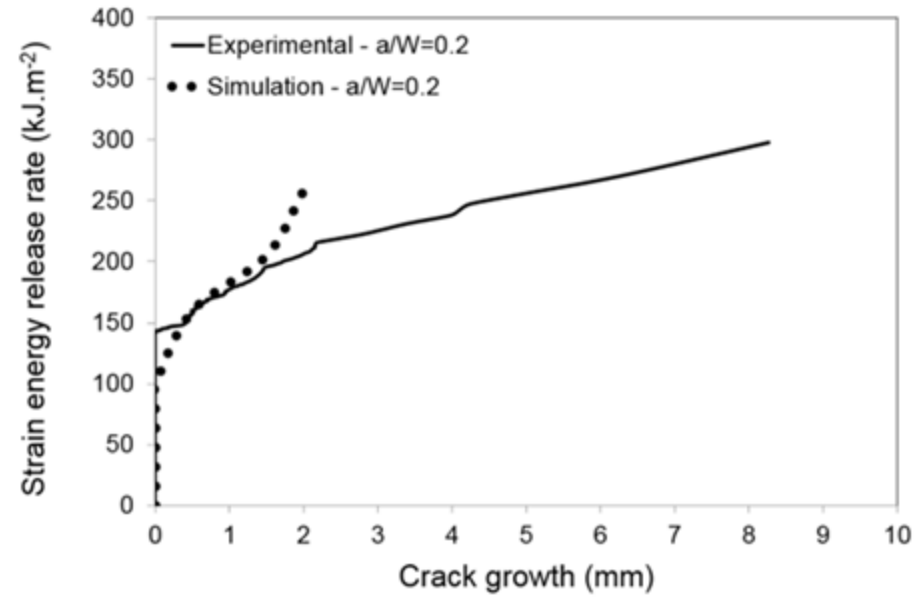
Mechanical properties					Viscoelastic parameters			Viscoplastic parameters		
$E_1(GPa)$	$E_2(GPa)$	$G_{12}(GPa)$	υ_{12}	$\tau_y(MPa)$	n_c	n_0	β_{44}	$\delta(MPa)$	K	N
56.5	56.6	1.35	0.04	10	4.05	6.9	0.6	400	$8.4e^{-12}$	9.5

Table 1. Parameters identification – mechanical properties, viscoelastic and viscoplastic parameters [20]